



A01-31227

AIAA 2001-2712

**Numerical Study of Unsteady Low-Reynolds-Number
Separation Bubbles Using a New High Order Scheme**

**Mahidhar Tatineni and Xiaolin Zhong
University of California, Los Angeles
Los Angeles, CA**

**31st AIAA Fluid Dynamics Conference and Exhibit
11-14 June , 2001 / Anaheim, CA**

NUMERICAL STUDY OF UNSTEADY LOW-REYNOLDS-NUMBER SEPARATION BUBBLES USING A NEW HIGH ORDER SCHEME

Mahidhar Tatineni* and Xiaolin Zhong†

University of California, Los Angeles, California 90095

Abstract

Low-Reynolds-number flows over airfoils are often characterized by the presence of separation bubbles, which can be unsteady with vortex shedding. The separation bubbles are unstable and their structure depends on the ambient disturbances present. Hence, it is important to understand the receptivity to disturbances and its effect on the separation bubbles. The objectives of this paper are two fold: 1) to develop and validate a new high-order (of arbitrarily high order) explicit finite difference scheme with stable boundary closure for solving the unsteady incompressible Navier-Stokes equations in the vorticity-velocity form; 2) to present results of numerical simulations of unsteady separation bubbles induced on a flat plate. The first part of this paper presents a new method for solving unsteady incompressible Navier-Stokes equations, which uses arbitrarily high-order finite difference schemes with stable boundary closure schemes derived directly on a non-uniform stretched grid. The second part of the paper presents results from separation bubble simulations, computed using a fifth order accurate method in the streamwise and wall normal direction and a spectral method in the spanwise direction. The separation bubbles on the flat plate are induced by specifying a velocity gradient in the freestream or by suction at the freestream. The freestream velocity distributions are varied to obtain different sizes of separation bubbles. The unsteady separation bubbles are studied by introducing wall blowing and suction disturbances, of varying frequencies and amplitudes.

1 Introduction

Low-Reynolds-number aerodynamics, in the range of $Re = 5 \times 10^4$ to 1×10^6 , is important for the design of a variety of aircrafts, ranging from sailplanes and human-powered aircrafts to high altitude unmanned aerial vehicles (UAV's).^[1,2] Low-Reynolds-number flows over airfoils are characterized by the presence of transitional separation bubbles.^[1] The structure of the separation

bubble is illustrated by a schematic in Fig. 1. The laminar flow separates due to the adverse pressure gradient. The separated boundary layer is unstable, and there is rapid growth of disturbances. The flow consequently becomes turbulent and reattaches. The region between the separation point and the reattachment point is called the separation bubble.

Computations of complex transitional separation bubble flows require high order schemes to resolve the wide range of spatial and temporal scales present in the flowfield. The first part of the paper presents a new high order scheme to solve the incompressible Navier-Stokes equations. Most finite difference schemes used in direct numerical simulation are either central difference schemes^[3,4] with filtering or upwind high-order schemes^[5-8]. The orders of accuracy of numerical methods used in practical DNS studies, however, are often limited to 6th-order or lower in the interior and 4th-order or lower on the boundary closure schemes because of the numerical instability of the boundary closure schemes. The main limiting factor in the application of high-order schemes is the numerical instability of high-order boundary closure schemes^[4,9,10]. The instability of high order boundary closure schemes often limits numerical schemes to 6th-order or lower in the interior and 4th-order or lower on the boundary closure schemes. In an earlier AIAA paper^[11] we proposed new arbitrarily high-order finite difference schemes which overcome the instability of high order boundary closure schemes by directly computing the derivative coefficients on a stretched non uniform grid. The numerical instability for high-order schemes based on uniform grids was shown to be due to the instability of polynomial interpolation based on uniform grids (the Runge phenomenon). The instability can be overcome for arbitrarily high-order finite difference schemes if the schemes are determined based on polynomial interpolation in the physical nonuniform grids. The amount of grid stretching is determined to maintain the stability of the overall schemes. In this paper we implement the new high order scheme for the incompressible Navier Stokes equations in the velocity-vorticity form.

The second part of the paper presents results from unsteady separation bubble simulations. Unsteady low-Reynolds-number separation bubbles have been the subject of many theoretical, experimental, and numeri-

*Graduate Student, Member AIAA.

†Associate Professor, Mechanical and Aerospace Engineering Department, Senior Member AIAA, xiaolin@seas.ucla.edu.

cal studies ^[12–21]. Early theoretical studies of separated flows revealed that the traditional boundary layer theory fails at the separation location due to a singularity in the boundary layer solution. ^[22] Stewartson, Smith and Kaups ^[13] developed a procedure based on the triple deck theory, which avoids such singularities, to study marginal separation problems. This method has been applied to unsteady three-dimensional ^[23] boundary layer flow. Hsiao and Pauley ^[24] did a quantitative study of the accuracy of triple deck and interactive boundary layer solutions at finite Reynolds-numbers. They found good agreement with numerical results at high Reynolds-numbers. Hence, for sufficiently gradual adverse pressure gradients the triple deck method and the interactive boundary layer method can be used to solve separation bubble problems. For unsteady problems, the nonlinear triple-deck system was developed by Vickers and Smith. ^[25] In their formulation additional equations are developed to resolve the detached shear layer far beyond the separation point. When combined with the triple deck formulation for the breakaway separation it enables a theoretical study of the unsteady separation and the inflexional modes associated with the detached shear layer.

Unsteady separation bubbles were first studied in detail by Gaster ^[12] through experimental measurements. A dimensionless pressure gradient parameter, $P_{avg} = \frac{\theta_{sep}^2}{\nu} \frac{\partial u_i}{\partial x_{sep}}$, was used in a criteria proposed by Gaster ^[12], based on experimental correlations, to predict the bursting of "short" separation bubbles to form "long" separation bubbles. In the expression $\frac{\partial u_i}{\partial x_{sep}}$ is the velocity gradient obtained from an inviscid analysis and θ_{sep} is the momentum thickness at the separation location. Based on experimental results Gaster showed that unsteadiness occurs for $P_{avg} < -0.24$. Experimental studies by Leblanc, Blackwelder, and Liebeck. ^[14] showed the presence of a dominant frequency in the velocity spectra in the separated region. The peak frequency was found to match the most amplified frequency calculated from linear stability theory. The linear evolution of disturbances in the separation bubble was also observed by Dovgal, Kozlov, and Michalke. ^[15] They also detailed the nonlinear interactions of the disturbances and the path to transition.

Two dimensional numerical simulations of Lin and Pauley ^[16] and our previous simulations ^[18,19] showed the unsteady nature of low-Reynolds-number separation bubbles and the associated vortex shedding. The numerical results showed that the growth of disturbance waves in the separated region leads to the vortex shedding. The dominant frequency from the numerical simulations is found to agree with the most unstable frequency from a linear stability analysis. Three dimensional effects in separation bubbles for flows over a flat plate have been studied by Hildings ^[21] and Rist and

Maucher. ^[20] Rist and Maucher introduced various 2-D and 3-D disturbances into the flowfield to study the non-linear disturbance development in the separation bubble. Their simulations were able to obtain a turbulent flowfield and predicted longitudinal vortices in the reattachment region. Their results showed that secondary disturbance amplification reduces considerably as the TS waves saturate, suggesting that the transition mechanism is not governed by secondary instability. They suggest an oblique breakdown mechanism for transition. Alam and Sandham ^[26] used direct numerical simulations of "short" laminar separation bubbles to show that the separated shear layer undergoes transition via oblique modes and vortex induced breakdown. Spalart and Strelets ^[27] numerically studied the transition process to show that the mechanism involves the instability of the shear layer producing Kelvin-Helmholtz vortices which breakdown. The results also show a flapping of the shear layer in the front part of the separation bubble which dominates in comparison to the convective disturbances. Maucher et. al. ^[28] showed that the definition of a well posed boundary condition at the freestream is critical. They proposed an interaction method based on thin airfoil theory to capture the displacement effects of the separation bubble on the surrounding potential flow. Zhang and Fasel evaluated the feasibility of flow control, by blowing and suction ahead of the separation bubble ^[29].

Past research, summarized above, has shown the complex nature of the unsteady low-Reynolds-number separation bubbles. The onset of unsteady vortex shedding, the question of absolute instabilities in large separation bubbles, feedback effects in separation bubbles, and bursting of separation bubbles are areas which still need to be studied. The parameters affecting the onset of vortex shedding and their influence on the transition process can be studied through detailed numerical simulations. This paper is focused on two objectives: 1) to develop high order schemes to effectively resolve the complex separated flowfields, and 2) to study the unsteady separation bubbles by varying the freestream velocity gradient, disturbance amplitude, and disturbance frequency.

2 Governing Equations and Numerical Methods

The new high order scheme for solving incompressible Navier-Stokes equations is detailed in this section. Current numerical methods used in most practical DNS studies are limited to 6th-order or lower in the interior and 4th-order or lower on the boundary because of the numerical instability of the boundary closure schemes. In an earlier AIAA paper ^[11] we showed that this numerical instability for high-order schemes based on uniform grids is due to the instability of polynomial interpolation based on uniform grids (the Runge phenom-

ena). This instability can be overcome for arbitrarily high-order finite difference schemes with stable boundary closure schemes if the schemes are derived directly on a non-uniform stretched grid. The details of governing equations and the new scheme are presented below.

Governing Equations

The flat plate separation bubble simulations are carried out using a time accurate incompressible Navier-Stokes solver. The formulation is based on the approach of Zhang and Fasel.^[29] The governing equations for this test case are the 3-D incompressible Navier-Stokes equations in the vorticity transport form:

$$\frac{\partial \omega_x}{\partial t} + \frac{\partial}{\partial y}(v\omega_x - u\omega_y) - \frac{\partial}{\partial z}(u\omega_z - w\omega_x) = \Delta \omega_x \quad (1)$$

$$\frac{\partial \omega_y}{\partial t} - \frac{\partial}{\partial x}(v\omega_x - u\omega_y) + \frac{\partial}{\partial z}(w\omega_y - v\omega_z) = \Delta \omega_y \quad (2)$$

$$\frac{\partial \omega_z}{\partial t} + \frac{\partial}{\partial y}(u\omega_z - w\omega_x) - \frac{\partial}{\partial z}(w\omega_y - v\omega_z) = \Delta \omega_z \quad (3)$$

where

$$\vec{\omega} = -\text{rot}(\vec{u})$$

$$\Delta = \frac{1}{Re} \frac{\partial^2}{\partial x^2} + \frac{\partial^2}{\partial y^2} + \frac{1}{Re} \frac{\partial^2}{\partial z^2}$$

and the nondimensionalization is as follows:

$$\begin{aligned} x &= \frac{x^*}{L}, \quad y = \sqrt{Re} \frac{y^*}{L}, \quad z = \frac{z^*}{L}, \\ u &= \frac{u^*}{U_\infty}, \quad v = \sqrt{Re} \frac{v^*}{U_\infty}, \quad w = \frac{w^*}{U_\infty} \end{aligned} \quad (4)$$

where the $*$'s represent the dimensional variables and $Re = U_\infty L/\nu$. The velocity components can be calculated from the following equations:

$$\frac{\partial^2 u}{\partial x^2} + \frac{\partial^2 u}{\partial z^2} = -\frac{\partial \omega_y}{\partial z} - \frac{\partial^2 v}{\partial x \partial y} \quad (5)$$

$$\Delta v = \frac{\partial \omega_x}{\partial z} - \frac{\partial \omega_z}{\partial x} \quad (6)$$

$$\frac{\partial^2 w}{\partial x^2} + \frac{\partial^2 w}{\partial z^2} = \frac{\partial \omega_y}{\partial x} - \frac{\partial^2 v}{\partial y \partial z} \quad (7)$$

Non-Uniform Grid High Order Finite Difference Method

The equations are discretized on a stretched grid in both directions, with the derivative coefficients computed directly for the nonuniform grid. The convective terms are discretized using a high order upwind finite difference scheme. The order can be set to an arbitrarily high number less than the number of grid points. The second derivatives in the viscous terms are discretized

directly on the stretched grid using high order finite differences. The details of the grid spacing and the explicit scheme are presented in the following subsections.

Grid Spacing

The stability of high-order schemes is dependent on the grid clustering near the boundaries. Spectral collocation methods utilizing the Chebyshev spacing are stable for arbitrary order schemes with boundary closure. However, this spacing is very restrictive on the timestep ($O(1/N^2)$) in a temporal integration of a PDE. In this paper we are using a less restrictive spacing with high-order finite difference schemes in order to maintain stability and high spatial accuracy and an $O(1/N)$ in minimum grid spacing and timestep.

In this paper, the grid spacing in the numerical simulations is controlled using the stretching function proposed by Kosloff and Tal-Ezer^[30] for a spectral method, i.e.,

$$x = \frac{\sin^{-1}(-\alpha \cos(\pi i/N))}{\sin^{-1} \alpha} \quad (8)$$

where the parameter α is used to change the stretching of the grid points from one limit of a Chebyshev grid at $\alpha \rightarrow 0$ and the other limit of an uniform grid at $\alpha=1$. Figure 2 shows a x vs. i/N plot for the stretching function ($N=101$). A grid stretching factor can be measured by $\Delta x_{min}/\Delta x_{uniform}$, where Δx_{min} is the minimum grid spacing in the stretching grid and $\Delta x_{uniform}$ is the average grid spacing. Figure 3 shows the grid stretching factor as a function of the stretching parameter α (for $N=51$).

Explicit Schemes

The coefficients for the explicit high order schemes on nonuniform grids are derived from a Lagrange polynomial interpolation. The interpolation polynomial is as follows:

$$P_n(x) = \sum_{j=1}^N l_j(x_i) f_j \quad (9)$$

Hence, the derivative at the point x_i can be calculated by differentiating the above polynomial as:

$$u'_i = \sum_{j=1}^N l'_j(x_i) f_j \quad (10)$$

where $l'_j(x_i)$ is calculated as follows: If $i \neq j$:

$$l'_j(x_i) = \prod_{l=1, l \neq j, l \neq i}^n (x_i - x_l)/a_j \quad (11)$$

If $i = j$:

$$l'_j(x_i) = \sum_{i=1, i \neq j}^n \left(\prod_{l=1, l \neq j, l \neq i}^n (x_i - x_l)/a_j \right) \quad (12)$$

where a_j is :

$$a_j = \prod_{l=1, l \neq j}^n (x_j - x_l) \quad (13)$$

Similarly, the second derivative is calculated as :

$$u''_i = \sum_{j=1}^N l''_j(x_i) f_j \quad (14)$$

Hence, once the x_i locations of the stencil are known the coefficients can be calculated explicitly using the above formulas.

In addition, the formulas for normal velocity derivatives on the wall include the first derivative at the wall (i.e. a compact scheme is used at the wall) to ensure that the continuity equation is satisfied. The solution is advanced in time using a fourth order Runge-Kutta method.

Boundary Conditions

The Blasius boundary layer solution is prescribed at the inlet. No slip conditions are used on the wall, except in the disturbance strip region where the normal velocity is specified. At the freestream, the streamwise velocity is specified and the vorticity is set to zero. The separation bubble is generated by prescribing a deceleration in the freestream velocity. Controlled disturbances can be introduced in the flowfield by blowing and suction at the wall upstream of the separation bubble. The disturbance form is as follows:

$$V_k(x, 0, t) = A_k \sqrt{Re} v_w(x) \sin(\beta t)$$

where $v_w(x)$ is the wall-forcing function, k is the fourier mode number (in the z direction) and β is the nondimensional frequency. $v_w(x)$ is zero everywhere except within the disturbance strip, where a point-symmetric amplitude distribution with respect to the center of the strip is used.

Numerical Scheme

The explicit nonuniform grid scheme detailed above is used for the spatial discretization of the governing vorticity equations. The discretized equations are advanced in time using a fourth order Runge-Kutta method. At each step of the method, once the vorticity field is computed, the velocity field needs to be solved. First, the wall normal component is solved using equation (6). The equation is discretized using the explicit

scheme detailed above. After fourier decomposition in the spanwise direction the algebraic equations for each spanwise wave number k are as follows:

$$\sum_{i=0}^{n_s-1} \alpha_i v_{i_s+i_j}^k + \sum_{j=0}^{m_s-1} \alpha_j v_{i_j+j_s}^k + v_{ij}^k(-k^2) = R_{ij}^k \quad (15)$$

where n_s, m_s are the stencil sizes for the derivative schemes. The solution is obtained using a line Gauss-Seidel method. Once the wall normal velocity is obtained the streamwise and spanwise velocities can be obtained by using a banded matrix solver at every streamwise grid location using equations (5), and (7). The wall vorticity components are calculated using the vorticity and velocity from the following equations:

$$\frac{\partial^2 \omega_x}{\partial x^2} + \frac{\partial^2 \omega_x}{\partial z^2} = - \frac{\partial^2 \omega_y}{\partial x \partial y} + \frac{\partial \Delta v}{\partial z} \quad (16)$$

$$\omega_y = 0 \quad (17)$$

$$\frac{\partial \omega_z}{\partial x} = \frac{\partial \omega_x}{\partial z} - \Delta v \quad (18)$$

3 Numerical Results

The high order code was validated by computing a Blasius boundary layer test case. The validated code is used for the simulations of the flat plate separation bubble test cases. The separation bubbles are induced by imposing velocity gradients in the freestream. The freestream velocity gradients are varied to change the size of the separation bubble, and to study the onset of unsteady vortex shedding. The unsteady characteristics are further studied by introducing disturbances upstream of the separation bubble. Results of 2-D simulations for cases with varying disturbance amplitudes and frequencies are presented.

3.1 New High Order Scheme

Blasius Boundary Layer Case

The high order incompressible explicit Navier-Stokes code was validated by computing a flat plate boundary layer test case. The flow variables are nondimensionalized as follows:

$$\begin{aligned} x &= \frac{x^*}{L}, \quad y = \sqrt{Re} \frac{y^*}{L}, \quad z = \frac{z^*}{L}, \\ u &= \frac{u^*}{U_\infty}, \quad v = \sqrt{Re} \frac{v^*}{U_\infty}, \quad w = \frac{w^*}{U_\infty} \end{aligned} \quad (19)$$

In this test case the Reynolds number is 10^5 and the characteristic length is $0.05m$. The domain ranges $x_o = 0.37$ to $x_N = 0.5$ in the x -direction and the maximum in the wall normal direction is $y_N = 18.84$. A 101×101 grid, with the grid stretching parameter $\alpha = 0.98$, is used for the calculations. Figure 4 shows

the grid distribution used in the calculations. The computations are carried out using 4th, 8th, 10th, and 16th order schemes. Figure 5 shows the variation of the wall normal velocity in the wall normal direction at $x = 0.469$ for the 16th order case. The solution is in very good agreement with the Blasius solution. The vorticity contours for the 16th order case are shown in Fig. 6. A comparison of the wall vorticity for the different order cases is shown in Fig. 7. Figure 8 shows a magnified view of Fig. 7. The magnified view shows that the solution agrees excellently for the 8th, 10th, and 16th order schemes.

Flat Plate Separation Bubble Case

The new high order scheme is used to compute the flat plate separation bubble test case of Rist and Maucher^[20] and the results are compared with the results from the existing fifth order code. In the test case the separation bubble is created by specifying a 8.8% drop in the streamwise freestream velocity. The grid stretching parameter $\alpha = 0.995$, with a 301×101 grid is used for the calculations. Figure 9 shows the comparison of the wall vorticity distribution for the two cases. The results show excellent agreement between the fifth order finite difference scheme and the new high order scheme with a eleven point stencil.

3.2 Flat Plate Separation Bubble Cases

The fifth order explicit Navier-Stokes code was used to compute the flat plate separation bubble test cases based on the approach of Rist and Maucher.^[20] In the test cases the separation bubble is created by specifying a jump in the streamwise freestream velocity. The flow variables are nondimensionalized as follows:

$$\begin{aligned} x &= \frac{x^*}{L}, \quad y = \sqrt{Re} \frac{y^*}{L}, \quad z = \frac{z^*}{L}, \\ u &= \frac{u^*}{U_\infty}, \quad v = \sqrt{Re} \frac{v^*}{U_\infty}, \quad w = \frac{w^*}{U_\infty} \end{aligned} \quad (20)$$

In this test case the Reynolds number is 10^5 and the characteristic length is $0.05m$. The domain ranges $x_o = 0.37$ to $x_N = 5.06$ in the x-direction and the maximum in the wall normal direction is $y_N = 18.84$. Test cases with velocity jumps of 8.8%, 8.9%, and 9%, and 9.5% from $x = 0.71$ to $x = 2.43$, are considered in the simulations. The separation bubble produced for the 8.8% case is shown in Figure 10. The wall vorticity distribution is shown in Figure 9. The zero vorticity locations correspond to the separation and reattachment points.

The mean flow from the 8.8%, and 8.9% velocity jump cases is chosen for the disturbance test cases. The 2-D disturbances were induced by blowing and suction upstream of the flow. The disturbance is induced at a blowing and suction strip from $x = 0.55$ to $x = 0.70$.

The disturbance form is as follows:

$$V(x, 0, t) = A\sqrt{Re}v_w(x)\sin(\beta t)$$

where $v_w(x)$ is the wall-forcing function, and β is the nondimensional frequency. $v_w(x)$ is zero everywhere except within the disturbance strip, where a point-symmetric fifth order polynomial amplitude distribution with respect to the center of the strip is used. All the test cases considered are tabulated in table 1.

Effect of disturbance amplitude

The effect of disturbance amplitudes is studied by varying the amplitudes from 5×10^{-8} to 1×10^{-3} for the 8.8% and 8.9% velocity drop cases. Figure 11 shows the variation of disturbance fourier amplitudes in the streamwise direction at $y = 0.1884\delta_s$ for the $A = 5 \times 10^{-8}$, and the 8.8% velocity drop case. The result shows that the disturbance growth is similar for all the modes and there are no nonlinear effects. Figure 12 shows the disturbance fourier amplitudes for the $A = 1 \times 10^{-4}$ case. In this case the higher modes are grow and saturate in the separation bubble, and the nonlinear effects can be seen. When the initial amplitude is further increased to $A = 1 \times 10^{-3}$ similar results are obtained as shown in Fig. 13. For the 8.9% velocity drop case a similar trend is observed. Figure 14 shows the disturbance fourier amplitudes in the streamwise direction at $y = 0.1884\delta_s$ for the $A = 5 \times 10^{-8}$ case. All the modes grow linearly through the separation bubble. Figure 15 shows the amplitudes for the $A = 1 \times 10^{-5}$ case. The presence of nonlinear effects can be clearly seen. For the $A = 1 \times 10^{-4}$ and $A = 1 \times 10^{-3}$ cases similar results are observed as shown in Figure 16 and Figure 17. In this case the disturbance growth is high enough to induce vortex shedding from the separation bubble. Figure 18 shows a sequence of instantaneous streamline plots to illustrate the resulting vortex shedding process.

Effect of disturbance frequency

The second set of calculations was done for a fixed amplitude and with varying frequencies. Figure 19 shows the disturbance amplitude growth with streamwise coordinate (x), for the flat plate separation bubble test case with $A = 5 \times 10^{-8}$, $\beta = 5.4$ and $\beta = 2.7$. The results show that the $\beta = 5.4$ leads to a much higher amplification of the disturbance. Hence, it is essential to study the stability characteristics of the separation bubble to find the most unstable disturbance frequency.

Effect of freestream velocity drop size

As discussed in the section on amplitude effects, a larger separation bubble (8.9% case) causes higher growth rates and leads to vortex shedding at lower dis-

turbance amplitudes. This is further illustrated by the 9.5% velocity drop case. In this case the numerical noise is enough to result in unsteady vortex shedding as shown in Figure 20. This is a possible explanation for unsteadiness in the numerical simulations by Pauley et. al. [31]. However, in cases with vortex shedding three dimensional effects will be very important. Three dimensional simulations are currently in progress to evaluate the effects.

4 Discussion of Results

The two dimensional simulations have shown that the vortex shedding process is initiated by the growth of disturbances in the separation bubble. For a sufficiently large separation bubble the numerical noise is enough for destabilization. This corresponds to the pressure gradient criteria proposed by Pauley et. al. [31]. This also a possible explanation for the bursting of the separation bubble reported by Gaster [12]. However, three dimensional effects are important in such transitional flows. For small separation bubbles Alam and Sandham [26] found that the three dimensional breakdown to turbulence is fundamentally different from the two dimensional simulation results. However, for high pressure gradients (or suction strengths) the two dimensional vortex shedding may dominate the breakdown process. Three dimensional simulations for high velocity drop cases are in progress to evaluate the shedding process and the bursting of short bubbles to form long bubbles.

5 Summary

An unsteady incompressible Navier-Stokes code, of arbitrarily high order on stretched grids, has been developed and verified by simulating a Blasius flow test case and a separation bubble test case. A fifth order code has been used to study separation bubble test cases. The separation bubble was found to be highly sensitive to the freestream velocity gradient imposed. The stability characteristics were studied by introducing disturbances by blowing and suction on the wall upstream of the separation bubble. The amplitudes and frequencies of the disturbances were varied. For high amplitude cases, the presence of nonlinear effects was seen, and the instabilities led to vortex shedding. The disturbance amplitude required to induce the shedding was found to reduce as the separation bubble size increased. For a sufficiently large separation bubble, the numerical noise was sufficient to induce the vortex shedding. Three dimensional simulations will be required to fully ascertain the effects of disturbances on the unsteady vortex shedding. The new high order scheme will be used for the proposed simulations.

6 Acknowledgments

This research has been supported by NASA Dryden Flight Research Center under Grant NCC 2-374.

References

- [1] Lissman, P., "Low Reynolds number airfoils," *Annual Review of Fluid Mechanics*, 1983, pp. 223-239.
- [2] Murray, J., Moes, T., K.Norlin, J.Bauer, Geenen, R., Moulton, B., and Hoang, S., "Piloted simulation study of a balloon-assisted deployment of an aircraft at high altitude." *NASA-TM 104245*, 1992.
- [3] Lele, S. K., "Compact Finite Difference Schemes with Spectral-like Resolution," *Journal of Computational Physics*, Vol. 103, 1992, pp. 16-42.
- [4] Pruet, C. D., Zang, T. A., Chang, C.-L., and Carpenter, M. H., "Spatial Direct Numerical Simulation of High-Speed Boundary-Layer Flows, Part I: Algorithmic Considerations and Validation," *Theoretical and Computational Fluid Dynamics*, Vol. 7, 1995, pp. 49-76.
- [5] Rai, M. M. and Moin, P., "Direct Numerical Simulation of Transition and Turbulence in a Spatially Evolving Boundary Layer," *Journal of Computational Physics*, Vol. 109, 1993, pp. 169-192.
- [6] Zingg, D. W., Lomax, H., and Jurgens, H., "High-Accuracy Finite-Difference Schemes for Linear Wave Propagation," *SIAM Journal of Scientific Comput.*, Vol. 17, No. 2, 1995, pp. 328-346.
- [7] Adams, N. A. and Shariff, K., "A High-Resolution Hybrid Compact-ENO Scheme for Shock-Turbulence Interaction Problems," *Journal of Computational Physics*, Vol. 127, 1996, pp. 27-51.
- [8] Zhong, X., "High-Order Finite-Difference Schemes for Numerical Simulation of Hypersonic Boundary-Layer Transition," *Journal of Computational Physics*, Vol. 144, August 1998, pp. 662-709.
- [9] Carpenter, M. H., Gotlieb, D., and Abarbanel, S., "The Stability of Numerical Boundary Treatments for Compact High-Order Finite-Difference Schemes," *Journal of Computational Physics*, Vol. 108, 1993, pp. 272-295.
- [10] Abarbanel, S. S., Chertock, A. E., and Yefet, A., "Strict Stability of High-Order Compact Implicit Finite-Difference Schemes: The Role of Boundary Conditions for Hyperbolic PDEs,I," *Journal of*

- Computational Physics*, Vol. Vol. 160, pp. 42–66, 2000.
- [11] Zhong, X. and Tatineni, M., “Stable High-Order Schemes and DNS of Boundary-Layer Stability on a Blunt Cone at Mach 8,” *AIAA Paper 2001-0437*, 2000.
- [12] Gaster, M., “The Structure and Behaviour of Laminar Separation Bubbles.” *AGARD-CP-4*, Vol. 2, 1966, pp. 813–854.
- [13] Stewartson, K., Smith, F., and Kaups, K., “Marginal Separation,” *Studies in Applied Mathematics*, Vol. 67, 1982, pp. 45–61.
- [14] LeBlanc, P., Blackwelder, R., and Liebeck, R., “A Comparison Between Boundary Layer Measurements in a Laminar Separation Bubble Flow and Linear Stability Theory Calculations,” *Perspectives in Turbulence Studies*, 1987, pp. 189–205.
- [15] Dovgal, A., Kozlov, V., and Michalke, A., “Laminar Boundary Layer Separation: Instability and Associated Phenomena,” *Progress in Aerospace Sciences*, Vol. 30, 1994, pp. 61–94.
- [16] Lin, J. M. and Pauley, L. L., “Low-Reynolds-Number Separation on an Airfoil,” *AIAA Journal*, Vol. 34(8), 1996, pp. 1570–1577.
- [17] Spalart, P. and Strelets, M., “Direct and Reynolds-Averaged Numerical Simulations of a Transitional Separation Bubble,” *Eleventh Symposium on Turbulent Shear Flows*, Institut National Polytechnique, Universite Joseph Fourier, 1997, pp. 30–13–30–18.
- [18] Tatineni, M. and Zhong, X., “Numerical Simulation of Unsteady Low-Reynolds-Number Separated Flows Over Airfoils,” *AIAA Paper 97-1929*, 1997.
- [19] Tatineni, M. and Zhong, X., “Numerical Simulations of Unsteady Low-Reynolds-Number Separated Flows Over the APEX Airfoil,” *AIAA Paper 98-0412*, 1998.
- [20] Rist, U. and Maucher, U., “Direct Numerical Simulation of 2-D and 3-D Instability Waves in a Laminar Separation Bubble,” *AGARD-CP-551*, 1994.
- [21] Hildings, C., “Simulation of Laminar and Transitional Separation Bubbles,” *Technical Reports from Royal Institute of Technology, Sweden*, Vol. Technical Report 1997:19, 1997.
- [22] Goldstein, S., “On laminar boundary-layer flow near a separation point,” *Quarterly Journal of Mech. Appl. Math*, Vol. 1, 1948, pp. 43–69.
- [23] Duck, P., “Three Dimensional Marginal Separation,” *Journal of Fluid Mechanics*, Vol. 202, 1989, pp. 559–575.
- [24] Hsiao, C. and Pauley, L., “The accuracy of the triple-deck theory for marginal separation,” *FED-Vol.149, Separated Flows, ASME*, 1993.
- [25] Vickers, I. and F.T.Smith, “Theory and computations for breakup of unsteady subsonic or supersonic separating flows,” *Journal of Fluid Mechanics*, Vol. 268, 1994, pp. 147–173.
- [26] Alam, M. and Sandham, N. D., “Direct Numerical simulation of short laminar separation bubbles with turbulent reattachment,” *Journal of Fluid Mechanics*, Vol. 403, 2000, pp. 223–250.
- [27] Spalart, P. and Strelets, M. K., “Mechanisms of transition and heat transfer in a separation bubble,” *Journal of Fluid Mechanics*, Vol. 403, 2000, pp. 329–349.
- [28] Maucher, U., Rist, U., and Wagner, S., “Refined Interaction Method for Direct Numerical Simulation of Transition in Separation Bubbles,” *AIAA Journal*, Vol. 38(8), 2000, pp. 1385–1394.
- [29] Zhang, H. and Fasel, H., “Numerical Investigation of The Evolution and Control of Two-Dimensional Unsteady Separated Flow Over a Stratford Ramp,” *AIAA Paper 99-1003*, 1999.
- [30] Kosloff, D. and Tal-Ezer, H., “A Modified Chebyshev Pseudospectral Method with an $O(1/N)$ Time Step Restriction,” *Journal of Computational Physics*, Vol. Vol. 104, pp. 457–469, 1993.
- [31] Pauley, L. L., Moin, P., and Reynolds, W., “The structure of two-dimensional separation.” *Journal of Fluid Mechanics*, Vol. 220, 1990, pp. 397–421.

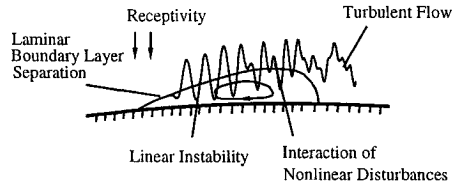


Table 1: List of unsteady separation bubble test cases considered. The freestream velocity drop, the disturbance amplitudes, and the disturbance frequency are varied

Figure 1: Structure of the separation bubble for low-Reynolds-number flows. A schematic detailing the growth of disturbances in various regions of the separation bubble.

Velocity Drop	Amplitude	Frequency
8.8%	5×10^{-8}	5.4
8.8%	1×10^{-4}	5.4
8.8%	1×10^{-3}	5.4
8.8%	5×10^{-8}	2.7
8.9%	5×10^{-8}	5.4
8.9%	1×10^{-5}	5.4
8.9%	1×10^{-4}	5.4
8.9%	1×10^{-3}	5.4
9.5%	Unsteady Vortex Shedding	-

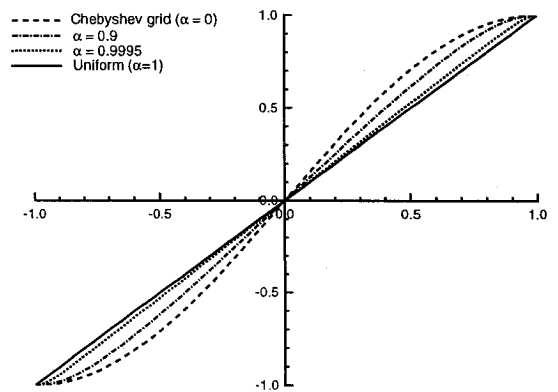


Figure 2: Grid stretching function used in this paper (x vs. i/N).

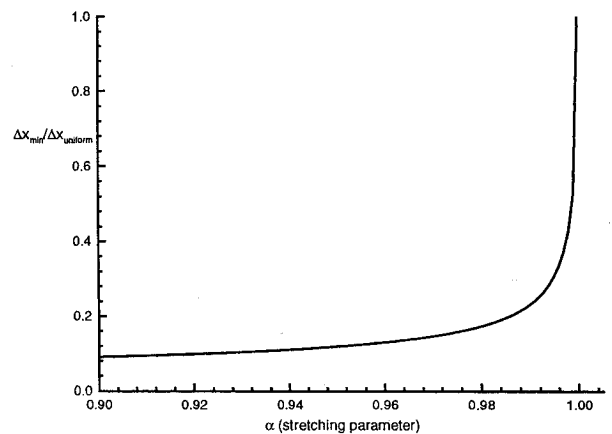


Figure 3: Grid stretching factor as a function of the stretching parameter α .

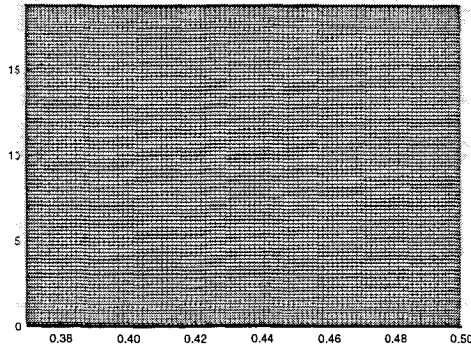


Figure 4: The 101×101 grid used for incompressible computations. The grid stretching parameter α is set to 0.98 in both directions.

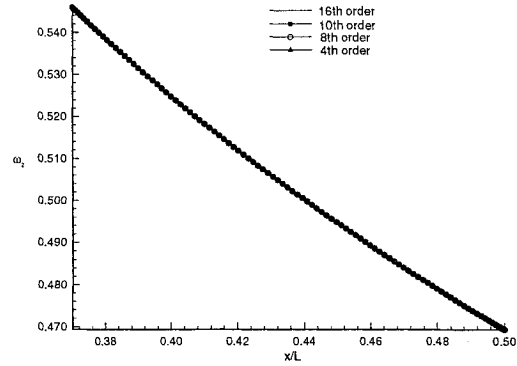


Figure 7: Comparison of the wall vorticity distribution computed using the 4th, 8th, 10th, and 16th order schemes.

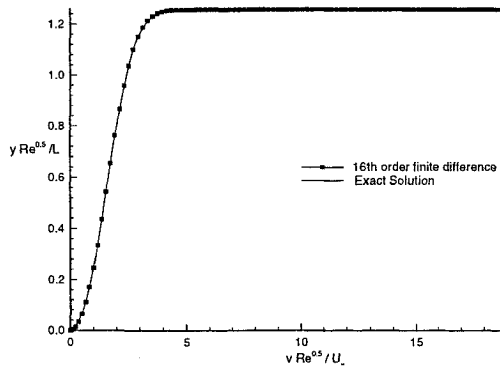


Figure 5: Comparison of the wall normal velocity numerical solution with the Blasius solution, at $x/L = 0.469$. The numerical solution is calculated using a 16th order scheme.

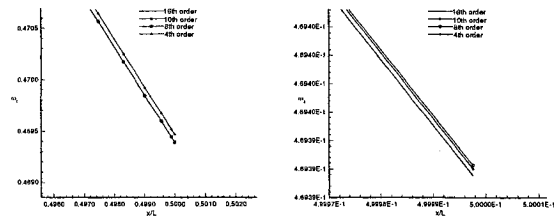


Figure 8: Comparison of the wall vorticity distribution computed using the 4th, 8th, 10th, and 16th order schemes. A magnified view near the end of the computational domain.

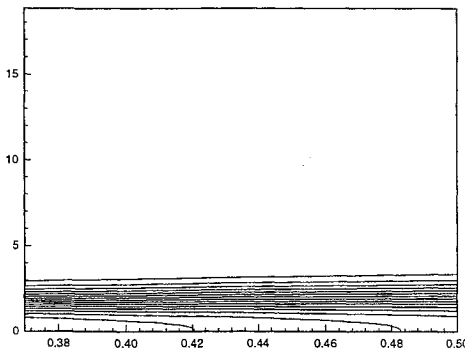


Figure 6: Spanwise vorticity contours for the incompressible flat plate boundary layer case. The numerical solution is calculated using a 16th order scheme.

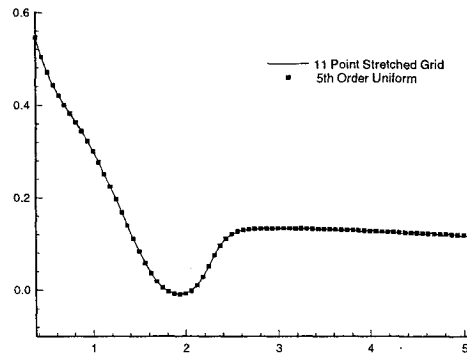


Figure 9: Comparison of the wall vorticity distribution, for the 8.8% velocity drop case, computed using a 11 point stencil (10th order) and the existing fifth order scheme.

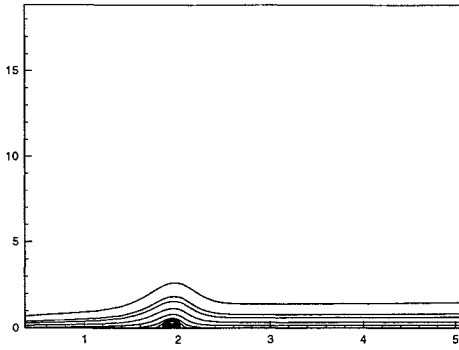


Figure 10: Mean flow streamlines showing the separation bubble for the 8.8% velocity drop case.

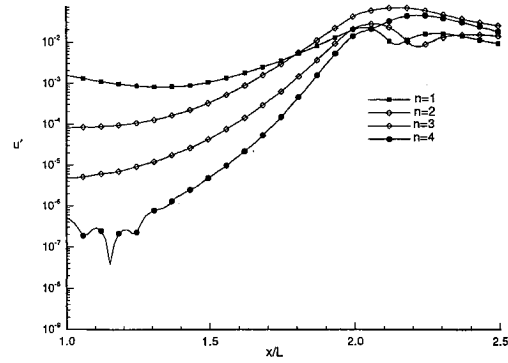


Figure 13: Variation of disturbance fourier amplitudes in the streamwise direction at $y = 0.1884\delta_s$. The wall blowing and suction amplitude is set to $A = 1 \times 10^{-3}$, and the freestream velocity drop is set to 8.8%.

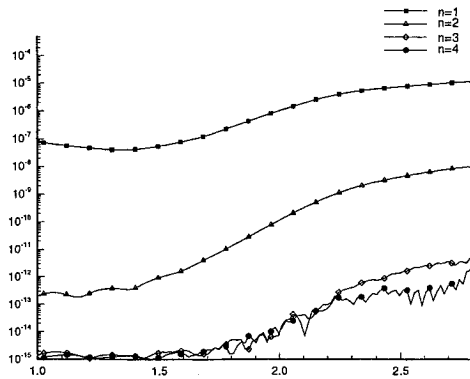


Figure 11: Variation of disturbance fourier amplitudes in the streamwise direction at $y = 0.1884\delta_s$. The wall blowing and suction amplitude is set to $A = 5 \times 10^{-8}$, and the freestream velocity drop is set to 8.8%.

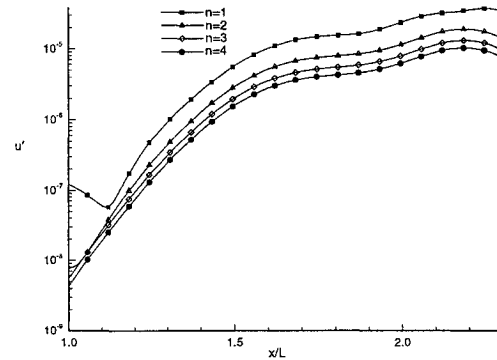


Figure 14: Variation of disturbance fourier amplitudes in the streamwise direction at $y = 0.1884\delta_s$. The wall blowing and suction amplitude is set to $A = 5 \times 10^{-8}$, and the freestream velocity drop is set to 8.9%.

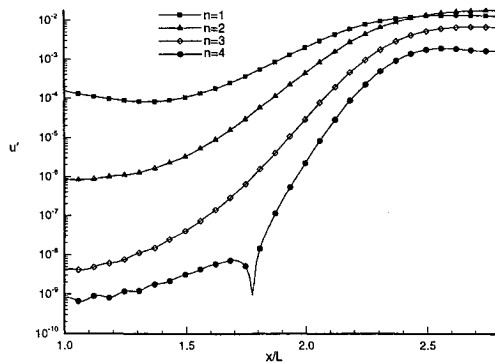


Figure 12: Variation of disturbance fourier amplitudes in the streamwise direction at $y = 0.1884\delta_s$. The wall blowing and suction amplitude is set to $A = 1 \times 10^{-4}$, and the freestream velocity drop is set to 8.8%.

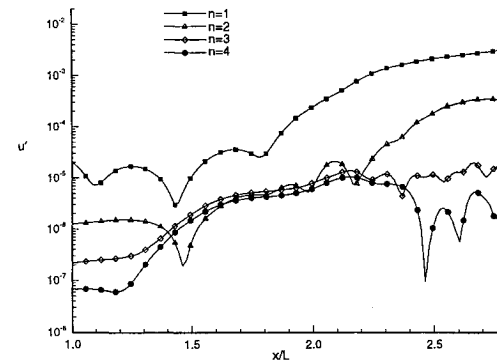


Figure 15: Variation of disturbance fourier amplitudes in the streamwise direction at $y = 0.1884\delta_s$. The wall blowing and suction amplitude is set to $A = 1 \times 10^{-5}$, and the freestream velocity drop is set to 8.9%.

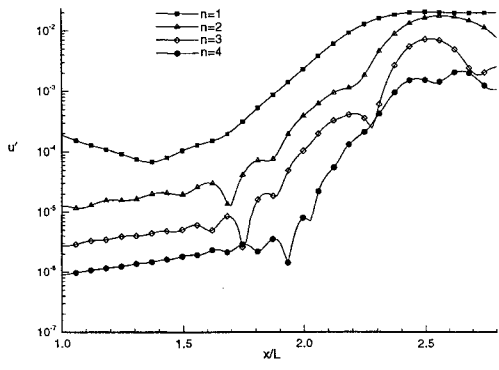


Figure 16: Variation of disturbance Fourier amplitudes in the streamwise direction at $y = 0.1884\delta_s$. The wall blowing and suction amplitude is set to $A = 1 \times 10^{-4}$, and the freestream velocity drop is set to 8.9%.

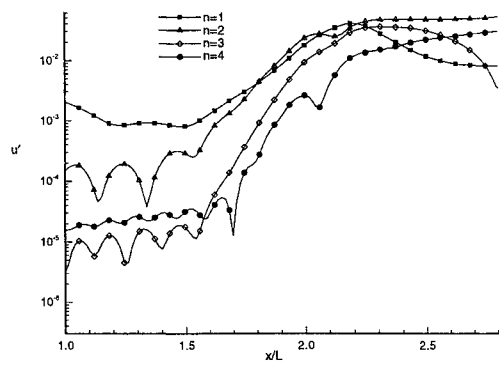


Figure 17: Variation of disturbance Fourier amplitudes in the streamwise direction at $y = 0.1884\delta_s$. The wall blowing and suction amplitude is set to $A = 1 \times 10^{-3}$, and the freestream velocity drop is set to 8.9%.

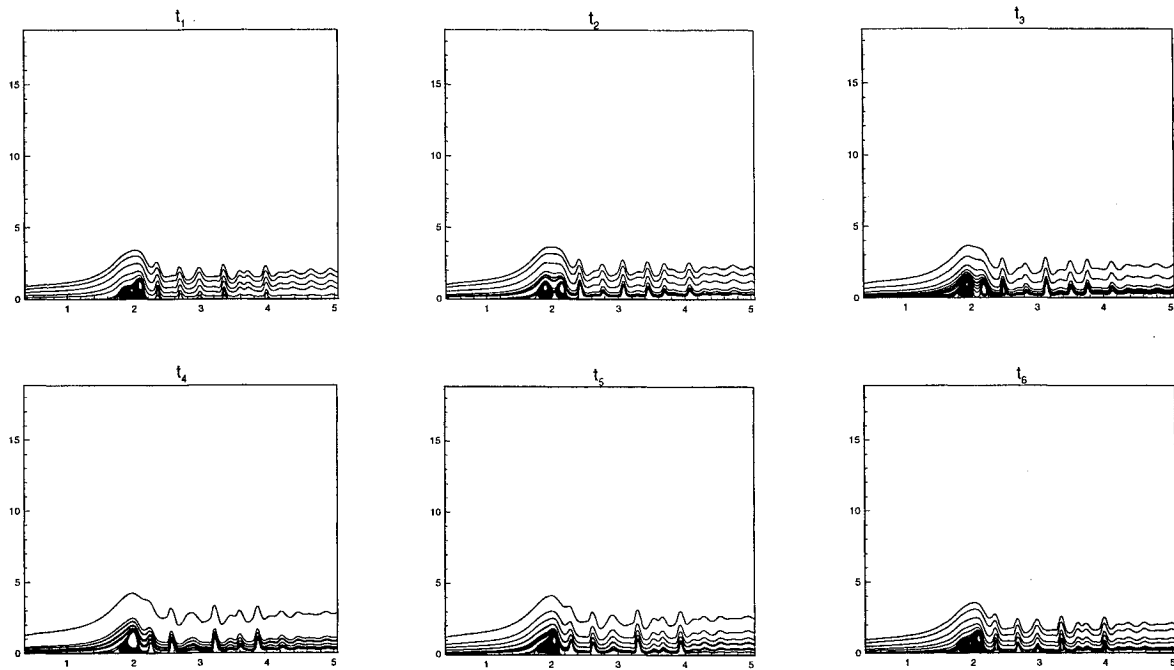


Figure 18: Flow field streamline plots, in sequence in time, showing the vortex shedding process for the flat plate separation bubble test case with $\beta = 5.4$, for the 8.9% velocity drop case with a disturbance amplitude of $A = 1 \times 10^{-4}$

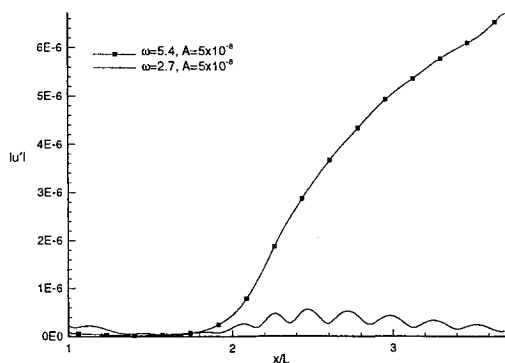


Figure 19: Disturbance amplitude growth with stream-wise coordinate (x), for the flat plate separation bubble test case for the 8.8% velocity drop case with $\beta = 5.4$ and $\beta = 2.7$. The Reynolds-number is 10^5 and the reference length $L = 0.05m$. The disturbances are introduced by blowing and suction at the wall upstream of the separation bubble.

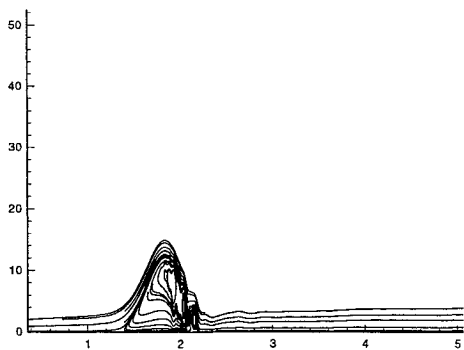


Figure 20: Flow field streamline plot for the 9.5% velocity drop case showing vortex shedding.